ISSN 1027-4510, Journal of Surface Investigation: X-ray, Synchrotron and Neutron Techniques, 2021, Vol. 15, No. 6, pp. 1154–1158. © Pleiades Publishing, Ltd., 2021.
Russian Text © The Author(s), 2021, published in Poverkhnost', 2021, No. 11, pp. 45–50.

Phase Transformations and Mechanical Properties of Two-Component Titanium Alloys after Heat Treatment in the Two-Phase Region (α + Intermetallic Compound) and High-Pressure Torsion

A. S. Gornakova[a, *], B. B. Straumal[a, b, **], Yu. I. Golovin[c], N. S. Afonikova[a], T. S. Pirozhkova[c], and A. I. Tyurin[c]

[a] *Osipyan Institute of Solid State Physics, Russian Academy of Sciences, Chernogolovka, Moscow oblast, 142432 Russia*
[b] *Chernogolovka Scientific Center, Russian Academy of Sciences, Chernogolovka, Moscow oblast, 142432 Russia*
[c] *Research Institute "Nanotechnology and Nanomaterials", Derzhavin Tambov State University, Tambov, 392000 Russia*
**e-mail: alenahas@issp.ac.ru*
***e-mail: straumal@issp.ac.ru*

Received April 19, 2021; revised June 20, 2021; accepted June 25, 2021

Abstract—In this paper, we measure the nanohardness (*H*) and Young's modulus (*E*) of three alloys: Ti–2.5 wt % Ni, Ti–2 wt % Cr, and Ti–2.2 wt % Fe preliminarily annealed in the two-phase region of the phase diagram (αTi + intermetallic compound) and then subjected to high-pressure torsion. The titanium alloy with the nickel addition showed the highest *H* and *E* values, they vary uniformly from the center to the edge of the sample, and the alloy after high-pressure torsion contains two phases: α and ω. The nanohardness of the alloy Ti–2.5 wt % Ni along the sample radius over the surface changes insignificantly: from minimal 4.8 to maximal 5.2 GPa, as does Young's modulus (from 121 to 155 GPa). The maxima of the *H* and *E* values fall in the middle of the sample radius. The alloy Ti–2.2 wt % Fe behaves differently: the presence of four phases α, β, ω, and TiFe leads to a strong scatter in the measured *H* and *E* values: from 4.4 to 2.0 GPa and from 131 to 12 GPa, respectively. Processing the *P*–*h* diagrams allows the nanohardness of the material to be related to its creep behaviour.

Keywords: titanium alloys, intermetallic compounds, high-pressure torsion, nanoindentation, Young's modulus, nanohardness, heat-treatment mode

DOI: 10.1134/S1027451021060082

INTRODUCTION

Interest in titanium and its alloys continues unabated [1–6]. These materials have a wide range of applications due to a successful combination of mechanical and technological characteristics [7, 8]. The nanomechanical properties of the materials are very important for the analysis of friction and abrasion processes. However, the regularities of the phase transformations in two-component α-titanium-based alloys strengthened by particles of intermetallic compounds, such as TiFe, Ti_2Ni, $TiCr_2$, under the action of shear deformation at high pressure are currently poorly studied and are of great interest. The presence of intermetallic compounds in the system, their properties and structure are determined by the position of the components in the periodic table, as well as by their atomic radii [9]. Nickel, iron, and chromium atoms can replace titanium atoms and form limited solid solutions with it. The TiFe intermetallic compound, which occupies a special place among hydride-forming alloys since it is capable of forming hydrides characterized by a dissociation pressure close to atmospheric at room temperature, was studied in detail [10]. The TiFe intermetallic compound has a cubic structure. Due to its strong hardening effect, iron is used in some titanium alloys as an alloying addition usually in amounts of 0.5–1.5%, although an alloy based on the β phase containing 5% Fe is known [11]. Interest in intermetallic compounds in the Ti–Ni system is caused by their many useful technological properties, such as plasticity, deformability in a wide temperature range, high mechanical strength, and shape memory effect [12]. In the Ti–Ni system, there are three intermetallic compounds: TiNi, Ti_2Ni, and $TiNi_3$ [13]. Ti_2Ni intermetallic compound is formed by a peritectic reaction and has a cubic structure. The hardening effect of titanium alloying with nickel at room temperature is small [11]. In terms of its effect on the polymorphic transformation of titanium, chromium belongs to strong β stabilizers. The solubility of chromium in α titanium does not exceed 0.5%. Chro-

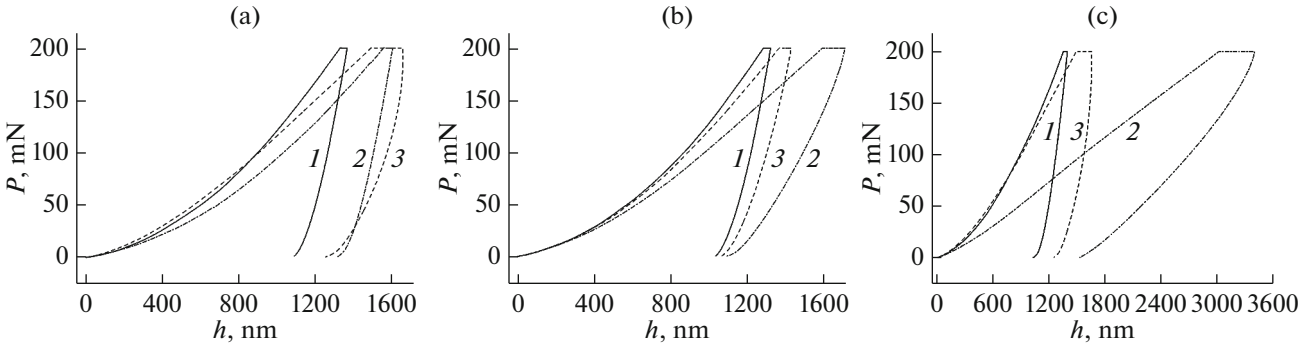

Fig. 1. *P–h* diagrams (*P* is the load value, *h* is the indentation depth) for: (a) center R_0, (b) the middle of the radius $R_{1/2}$, (c) edges R_1 of the samples (*1*) Ti–2.5 wt % Ni, (*2*) Ti–2.2 wt % Fe, and (*3*) Ti–2 wt % Cr.

mium provides high strength in alloys with titanium at good ductility and increases the efficiency of hardening heat treatment [11]. However, at elevated temperatures, the β phase eutectically decomposes, accompanied by the precipitation of $TiCr_2$ and, consequently, the loss of plasticity. At temperatures below 1150°C, $TiCr_2$ has a face-centered cubic (FCC) lattice. $TiCr_2$ intermetallic compound is highly fragile. Its presence in alloys even in small amounts sharply reduces their ductility. This paper is aimed at studying the effect of high-pressure torsion and the fraction of an intermetallic compound on the phase transformations, nanohardness, and Young's modulus in Ti–2.5 wt % Ni, Ti–2 wt % Cr, and Ti–2.2 wt % Fe alloys.

METHODS

Two-component titanium alloys Ti–2.5 wt % Ni, Ti–2 wt % Cr, and Ti–2.2 wt % Fe were obtained from titanium TI-1 (iodide titanium 99.98%), chromium (99.99%), iron (99.97%), and nickel (99.95%). The alloys were prepared in an induction furnace in a pure argon atmosphere. The resulting alloy ingots were structurally and chemically homogeneous along their entire length and thickness. The disks with a thickness of 0.7 mm were cut from cylindrical alloy ingots with a diameter of 10 mm. Then, the samples were sealed in quartz ampoules with a residual pressure of 4×10^{-4} Pa. After annealing, the samples were quenched in water together with the ampoule. The Ti–Ni and Ti–Cr alloys were annealed at 600°C (2774 h), and the Ti–Fe alloy was annealed at 470°C (673 h). The obtained samples were subjected to high-pressure torsion (HPT) at room temperature, 7 GPa, a strain rate of 1 rpm, and 5 revolutions of a plunger. After HPT, the thickness of the samples was 0.35 mm. The nanohardness of the sample surface was measured using a TI-950 Triboindenter equipped with a Berkovich indenter. The measurements were performed at the center (R_0), in the middle of the radius ($R_{1/2}$), and near the edge (R_1) of the samples, and the loading rate was constant: $dP/dt = 40$ mN/s. Before measurements, the surface of the samples was polished with a diamond paste with a grain size of 1 μm. The numerical values of the nanohardness (*H*) and Young's modulus (*E*) of the studied samples were calculated using the Oliver-Pharr method [14–16] based on the characteristic *P–h* diagrams (Fig. 1), where *P* is the load value, and *h* is the indentation depth. The studies were carried out at room temperature and a constant maximal load applied to the indenter: $P_{max} = 200$ mN. The *H* and *E* values were obtained by averaging the results of 12 independent experiments. Phase analysis of the samples was performed using a Siemens D-500 X-ray diffractometer ($CuK_{\alpha 1}$ radiation). The lattice parameters were calculated using the PowderCell program for Windows V.2.4.08.03.2000. To determine the chemical composition of the samples, we used a Supra 50VP high-resolution scanning electron microscope with an INCA Energy+ microanalysis system equipped with an Oxford Instruments attachment for energy dispersive microanalysis.

RESULTS AND DISCUSSION

Phase Composition of the Samples before and after HPT

The phase composition of the three studied alloys is presented in Table 1. The bulk of the material is in the α-Ti phase. Compared with the lattice parameters of the α phase of pure titanium in two-component alloys, the lattice parameter *a* is smaller, and, therefore, the *c/a* ratio is larger. The cell in the *hcp* lattice in two-component alloys is "compressed", i.e., titanium is enriched in the second component, so the lattice period decreased. The phase composition after annealing in the three studied alloys differs in terms of the fraction and type of the intermetallic structure.

Table 2 shows data on the volume fraction of each phase and the lattice parameters of these phases after annealing and HPT obtained from the entire surface of the samples. All three samples differ in terms of the phase composition. In the titanium alloy with nickel, there are only two phases: α and ω. An intermetallic compound was also found in the alloy with chromium.

Table 1. Lattice parameters, phases, and their content in the alloys after heat treatment in the αTi + intermetallic compound region.

Alloy	Phase-diagram region	αTi		TiMe	
		volume fraction	*a*, *c*, nm	volume fraction	*a*, nm
Ti–2.5 wt % Ni	αTi + Ti_2Ni	96	0.2944, 0.4688	4	1.1318
Ti–2 wt % Cr	αTi + $TiCr_2$	98	0.2950, 0.4689	2	0.6933
Ti–2.2 wt % Fe	αTi + TiFe	97	0.2950, 0.4687	3	0.2978
Pure Ti	–	–	0.2955, 0.4686	–	–

Table 2. Lattice parameters, phases, and their content in the alloys after heat treatment and high-pressure torsion.

Alloy	αTi		βTi		ωTi		TiMe	
	volume fraction	*a*, *c*, nm	volume fraction	*a*, nm	volume fraction	*a*, *c*, nm	volume fraction	*a*, nm
Ti–2.5 wt % Ni	37	0.2951, 0.4688	–	–	63	0.4625, 0.2812	–	–
Ti–2 wt % Cr	43	0.2950, 0.4690	–	–	55	0.4628, 0.2813	2 ($TiCr_2$)	0.6943
Ti–2.2 wt % Fe	8	0.2950, 0.4690	16	0.3255	76	0.4626, 0.2814	≥2 (TiFe)	0.2979
Pure Ti	–	0.2959, 0.4690	–	–	–	0.4627, 0.2830	–	–

Alloying titanium with iron in combination with HPT leads to the formation of four phases: α, β, ω, and TiFe. It is possible that a large fraction of the intermetallic compound in the alloy after annealing leads to more uniform distribution of the material and, consequently, to close values of the nanohardness and Young's modulus after HPT at the center and edge of the sample.

Nanohardness of the Alloys

For the Ti-Ni alloy, the values of the nanohardness *H* varied slightly: from 4.8 ± 0.1 at the center to 5.0 ± 0.1 GPa at the edge of the sample (Fig. 2) while the values of Young's modulus varied from 148 to 121 GPa. For the Ti–Fe and Ti–Cr alloys, the scatter in the values of the nanohardness and Young's modulus was wider. We consider in more detail three areas of sample measurement: at R_0, $R_{1/2}$, and R_1 for each alloy. The nanohardness values in the central part of the samples of the alloys with nickel and iron differ by 1.3 ± 0.2 GPa. Since the central region of the sample is known to be least of all subjected to deformation, one can assume that the Ti–Ni alloy was initially harder than Ti–Fe. At the middle of the radius, the scatter of the nanohardness values for the three alloys is the lowest for the sample: 0.8 GPa. This region undergoes more severe deformation, which "levels out" the nanohardness of the samples. At the edge of the samples, the strongest scatter of the nanohardness values is observed: 2.9 GPa. The central part of the sample and its edge are usually not used for further research, but one would still like to understand what causes such a scatter of values. The first assumption: the size of the groove under the plunger is 0.3 mm, and the thickness of the initial sample varied from 0.6 to 0.7 mm. It is possible that variations in the thickness of the initial samples, which affect the degree of shear deformation, played a negative role and led to a scatter of the values at the edges. The second assumption is that there is insufficient qualitative preparation of the sample surface before measurements, which led to the scatter of data. Both of these are possible, while the error should be the same in the measurements since HPT and surface preparation were performed in the same way. There is another more significant assump-

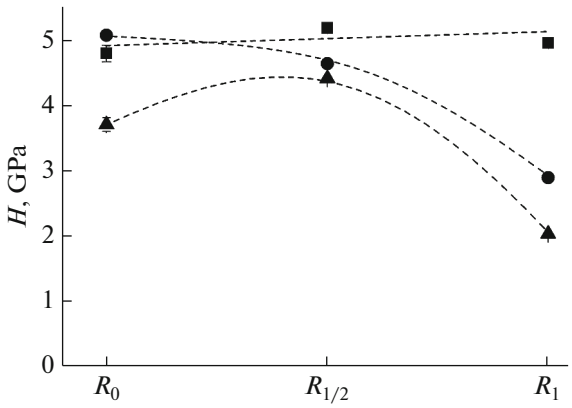

Fig. 2. Dependence of the nanohardness of Ti–2.5 wt % Ni (squares), Ti–2.2 wt % Fe (triangles), and Ti–2 wt % Cr (circles) preliminarily annealed and subjected to high pressure torsion on the measurement area over the sample surface: at the center (R_0), in the middle of the radius ($R_{1/2}$), and at the edge (R_1).

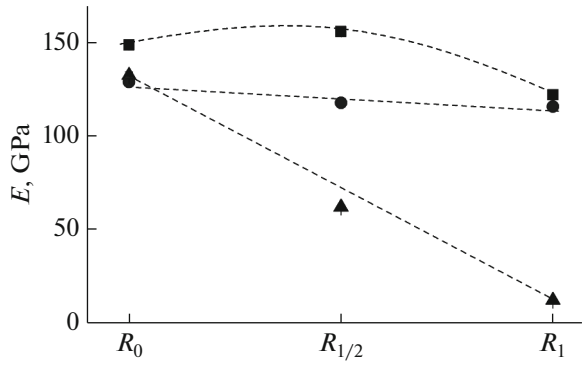

Fig. 3. Dependence of Young's modulus for the alloys Ti–2.5 wt % Ni (squares), Ti–2.2 wt % Fe (triangles), and Ti–2 wt % Cr (circles) on the measurement location over the sample surface: at the center (R_0), the middle of the radius ($R_{1/2}$), and the edge (R_1). The samples were preliminarily annealed and subjected to high-pressure torsion.

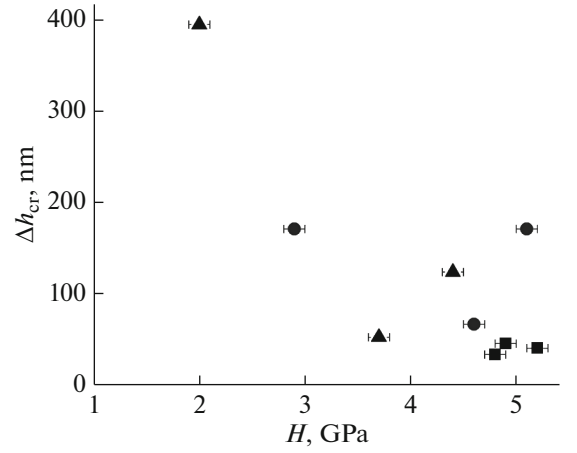

Fig. 4. Dependence of the increase in the indentation depth (Δh_{cr}) during creep on the nanohardness of samples of the alloys Ti–2.5 wt % Ni (squares), Ti–2.2 wt % Fe (triangles), and Ti–2 wt % Cr (circles) after high-pressure torsion.

tion, which was not tested in this study: the phase composition of the samples in the three regions and microstructural components, such as the size or fraction of phases or the size of phase particles or the fraction of interphase boundaries and the "precipitation" of intermetallic particles at grain boundaries. These assumptions open up the possibility of further, more detailed research.

Young's Modulus of the Alloys

We consider the measured values of Young's modulus (E) (Fig. 3). As can be seen, in the central part of the samples, the difference in the E values of the alloys is less than 20 GPa while the scatter is more than 100 GPa at the edges. It can be assumed that the scatter is due to the fact that the elasticity modulus is a more sensitive characteristic, and the presence of small irregularities on the surface and grain boundaries can make its own adjustments to the mechanisms of plasticity. However, the uniformity of sample preparation precludes this assumption. The combination of α- and ω phases produces the highest values of nanohardness and Young's modulus and, what is important, a uniform distribution of these values from the center to the edge of the sample in the Ti-Ni alloy. Such a spread in the H and E values was not discussed in publications [17–20], and therefore, the obtained data are of undoubted interest.

Features of the P-h Diagrams

A strong difference in the Δh_{cr} regions, which are responsible for the increment in the indentation depth during creep, was noted on the *P-h* diagrams recorded during the experiment (Fig. 1). Having calculated the Δh_{cr} values from Fig. 1, we plotted the dependence of the increment in the indentation depth (Δh_{cr}) during creep on the nanohardness for the studied alloys after HPT (Fig. 4). The resulting dependence demonstrates how unevenly the components are mixed in the samples during HPT. The alloy with nickel has the same Δh_{cr} values along the entire sample while the Δh_{cr} values are very different for the alloys with chromium and iron. Another feature was that different values of the nanohardness were observed for the alloy with chromium at the same value of Δh_{cr}. This behavior may be due to inhomogeneity of the sample itself, i.e., the indenter hit either the grain boundary or the interface or another phase.

CONCLUSIONS

The nanohardness and Young's modulus were measured for Ti–2.5 wt % Ni, Ti–2 wt % Cr, and Ti–2.2 wt % Fe alloys preliminarily annealed in the two-phase region (αTi + intermetallic compound) and subjected to high-pressure torsion. The alloy Ti–2.5 wt % Ni with a high content of the intermetallic phase showed higher values of the nanohardness and Young's modulus after HPT. Nanoindentation is a suitable tool for studying microinhomogeneities of the structure and composition that arise during HPT.

ACKNOWLEDGMENTS

We are deeply grateful to M. I. Egorkin (LPCBC at the ISSP, RAS) for the manufacture of titanium alloys and A. R. Kilmametov (Institute of Nanotechnology at the KIT, Karlsruhe, Germany) for processing samples under high-pressure torsion.

FUNDING

This work was partially carried out within the framework of the state assignment of the Osipyan Institute of Solid State Physics, Russian Academy of Sciences and was supported by the Russian Foundation for Basic Research, projects no. 18-29-17047 and no. 19-58-06002, as well as by Derzhavin Tambov State University, grant no. 591-3, February 25, 2020.

CONFLICT OF INTEREST

The authors declare that they have no conflict of interest.

REFERENCES

1. M. S. Asl, S. A. Delbari, M. Azadbeh, et al., J. Mater. Res. Technol. **9**, 10647 (2020). https://doi.org/10.1016/j.jmrt.2020.07.066
2. N. Moshokoa, L. Raganya, B. A. Obadele, R. Machaka, and M. E. Makhatha, Int. J. Adv. Des. Manuf. Technol. **111**, 1237 (2020). https://doi.org/10.1007/s00170-020-06208-7
3. L. Verestiuc, M.-C. Spataru, M. S. Baltatu, et al., J. Mech. Behav. Biomed. Mater. **113**, 104198 (2021). https://doi.org/10.1016/j.jmbbm.2020.104198
4. G. Deng, T. Bhattacharjee, Y. Chong, et al., J. Alloys Compd. **822**, 153604 (2020). https://doi.org/10.1016/j.jallcom.2019.153604
5. Y. Chong, G. Deng, A. Shibata, and N. Tsuji, Adv. Eng. Mater. **21**, 1900607 (2019). https://doi.org/10.1002/ADEM.201900607
6. Y. L. Kao, G. C. Tu, C. A. Huang, and T. T. Liu, Mater. Sci. Eng., A **398**, 93 (2005). https://doi.org/10.1016/j.msea.2005.03.004
7. C. Veiga, J. P. Davim, and A. J. R. Loureiro, Rev. Adv. Mater. Sci. **32**, 133 (2012).
8. G. Lütjering and J. C. Williams, *Titanium*, 2nd ed. (Springer, Berlin, 2007).
9. Intermetallics. https://bigenc.ru/chemistry/text/2014495.
10. M. Yu. Zadorozhnyi, Candidate's Dissertation in Engineering (Moscow Inst. Steel Alloys, Moscow, 2013).
11. Titanium. http://www.libmetal.ru/titan/titan%203.htm.
12. T. M. Kulikova, G. K. Moiseev, and N. I. Il'inykh, Izv. Chelyabinsk. Nauchn. Tsentra, No. **1**, 41 (2001).
13. J. L. Murray, Bull. Alloy Phase Diagrams **2**, 320 (1981).
14. W. C. Oliver and G. M. Pharr, J. Mater. Res. **19**, 3 (2004). https://doi.org/10.1557/jmr.2004.19.1.3
15. Yu. I. Golovin, A. I. Tyurin, E. G. Aslanyan, T. S. Pirozhkova, and V. M. Vasyukov, Phys. Solid State **59**, 1803 (2017). https://doi.org/10.1134/S1063783417090104
16. Yu. I. Golovin, A. I. Tyurin, and Yu. L. Iunin, Dokl. Phys. **48**, 505 (2003). https://doi.org/10.1134/1.1616061
17. G. Deng, T. Bhattacharjee, Y. Chong, et al., J. Alloys Compd. **82**, 153604 (2020). https://doi.org/10.1016/j.jallcom.2019.153604
18. M. Nie, C. T. Wang, M. Qu, et al., J. Mater. Sci. **49**, 2824 (2014). https://doi.org/10.1007/s10853-013-7988-z
19. A. S. Gornakova, A. B. Straumal, I. I. Khodos, I. B. Gnesin, A. A. Mazilkin, N. S. Afonikova, and B. B. Straumal, J. Appl. Phys. **125**, 082522 (2019). https://doi.org/10.1063/1.5053937
20. B. B. Straumal, A. Korneva, A. R. Kilmametov, L. Litynska-Dobrzynska, A. S. Gornakova, R. Chulist, M. I. Karpov, and P. Zieba, Materials **12**, 426 (2019). https://doi.org/10.3390/ma12030426

Translated by A. Ivanov